# Supporting Information for "Adoptive CD8+T-cell grafted with liposomal immunotherapy drugs counteract immune suppressive tumor microenvironment to elicit enhanced therapy on melanoma"

Simeng Liu ‡ [a], Huimin Liu‡ [a], Xiaoshuang Song‡ [a], Ailing Jiang [a], Yuchuan Deng [a], Chengli Yang [a], Dan Sun [a], Kun Jiang [c], Fan Yang [b], Zheng Yu [a,*]

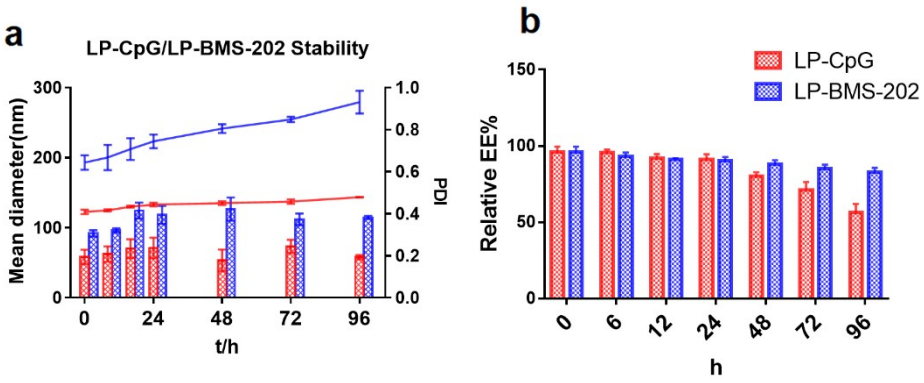


Figure S1 Stability of LP-CpG and LP-BMS-202

(a) Change of particle size and PDI of LP-CpG and LP-BMS-202 during storage at 4 °C, blue line: mean; (b) Change of entrapment efficiency (EE) of LP-CpG and LP-BMS-202 over storage time at 4 °C;

| Samples | Loading efficiency (mg/mg) | Encapsulate efficiency (EE) | Particle Size (nm) | PDI | Zeta potential (mV) |
|---|---|---|---|---|---|
| Anionic LP | | | 85.5±2.3 | 0.29±0.05 | -38.7±4.2 |
| Cationic LP | | | 124.7±3.4 | 0.231±0.04 | +39.0±5.4 |
| MPB-LP | | | 95.5±2.3 | 0.19±0.03 | -40.7±2.2 |
| LP-CpG | 10% | 90±4% | 205.0±4.2 | 0.33±0.23 | -43.6±3.2 |
| LP-BMS-202 | 10% | 95±4% | 122.3±3.5 | 0.173±0.12 | -43.0±3.4 |

Table S1. Characteristics of the optimized liposome formulations.

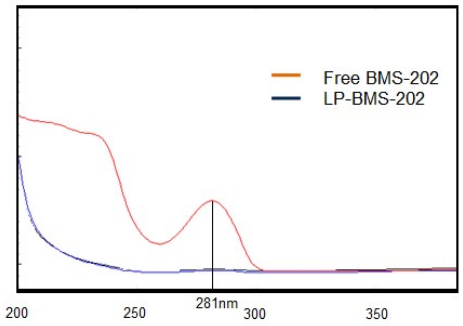


Figure S2. UV-vis spectra of free BMS-202 and LP-BMS-202.

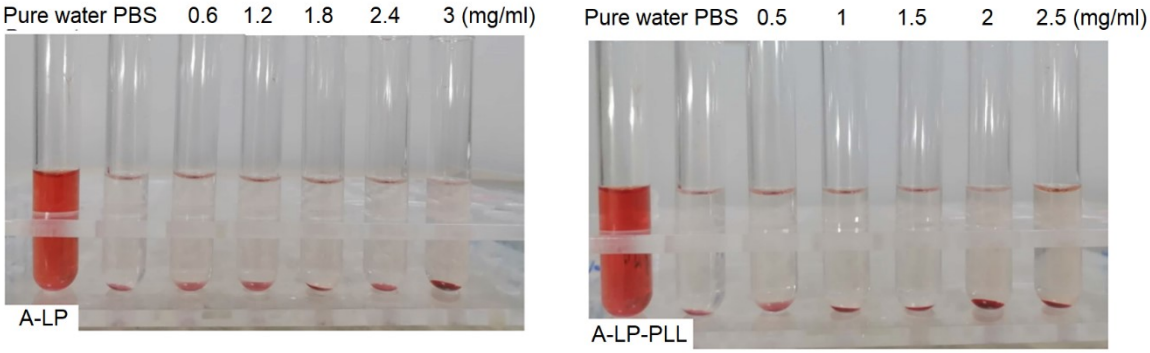


Figure S3. Photographs of hemolysis rate for A-LPs with various lipid concentrations.

The degree of hemolysis was determined by measuring hemoglobin concentration, and the hemolysis rate less than 5% relative to positive control indicates good hemocompatibility of the liposomes.

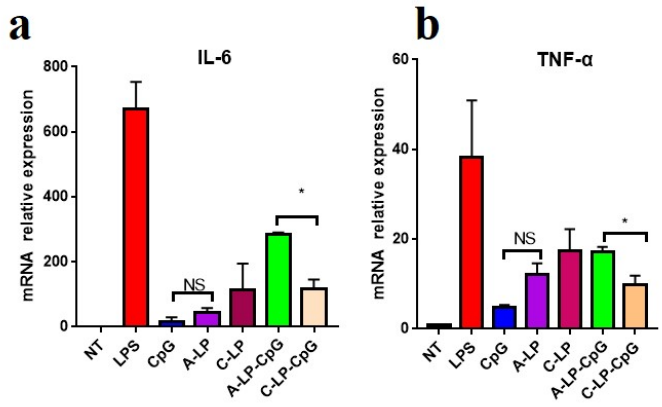


Figure S4. mRNA expression of IL-6(a) and TNF-α(b) in DC2.4 after treatment of

various samples including PBS as negative control (NT), LPS as positive control (LPS), blank liposomes (A-LP/C-LP), free CpG (CpG), A-LP-CpG and C-LP-CpG; Data are expressed as mean ± SD of each group (n = 3). * $p < 0.05$.

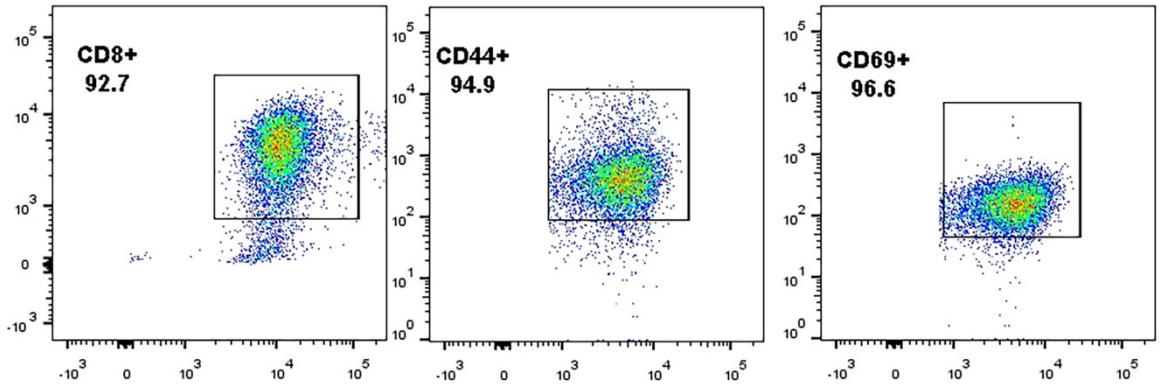


Figure S5. Surface marker of activated $CD8^{+}$T cell after culture for 48h with CD3/ CD28 antibody.

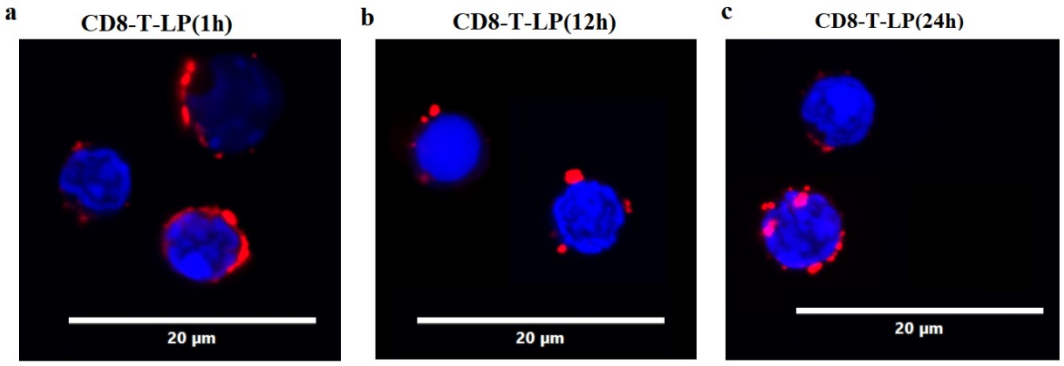


Figure S6.T-cell conjugated with DiD labeled anionic liposomes cultured for various time points including 1h (a), 12h (b) and 24h (c).

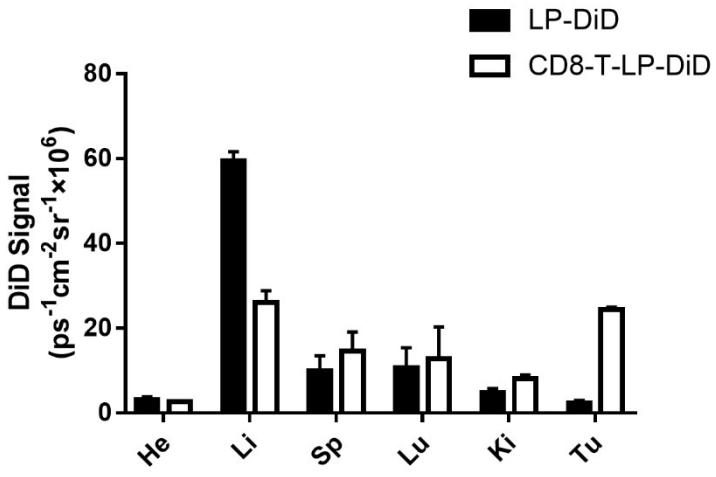


Figure S7. Distribution of LP and CD8-T-LP in the main organs of mice at 24-hour after administration.

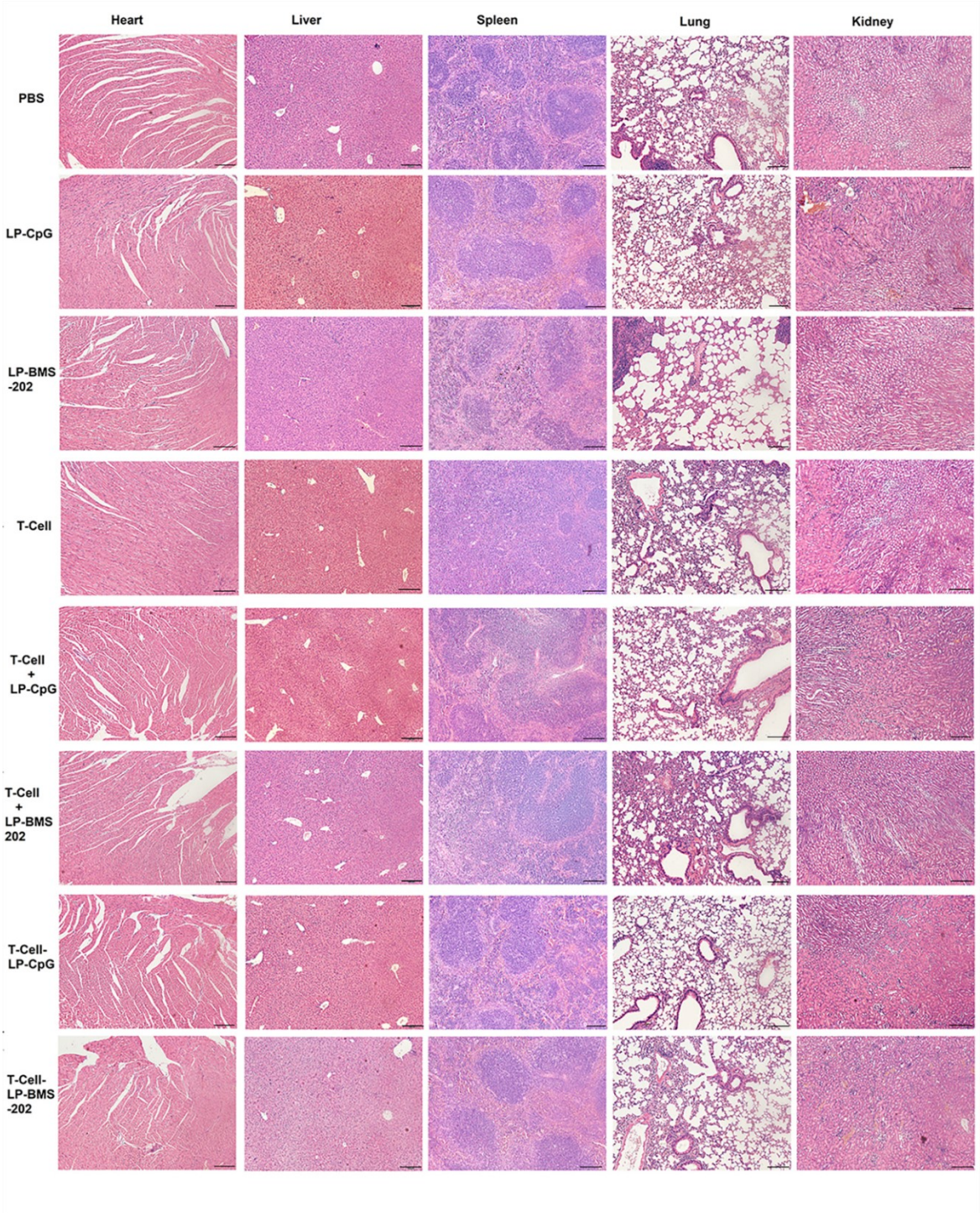


Figure S8. Representative histological HE staining photographs of the main organs after the treatment of the following groups including PBS, LP-CpG, LP-BMS-202, CD8-T, CD8-T+LP-CpG, CD8-T+LP-BMS-202, CD8-T-LP-CpG, CD8-T-LP-BMS-202. The scale bar represents 100 μm.

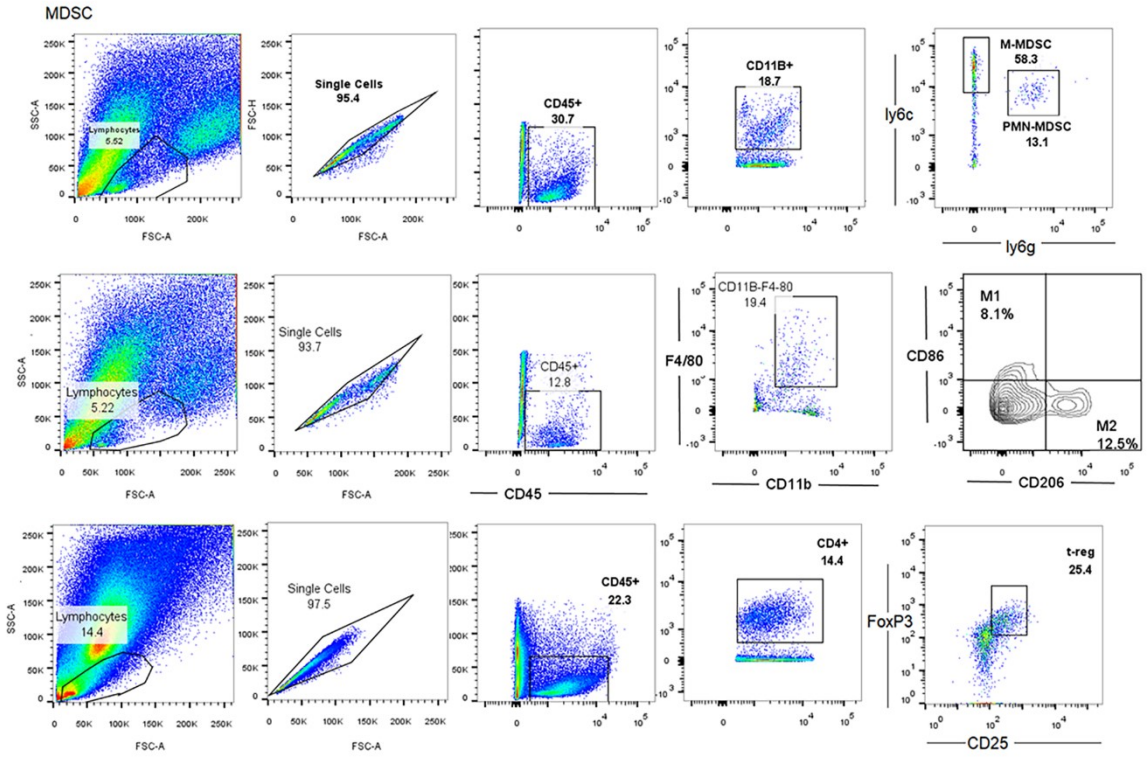


Figure S9. Flow cytometry gating strategy for the subgroups of cells including M-MDSC (CD45+ CD11b+ Ly6C$^{high}$ Ly6G−), PMN-MDSC (CD45+ CD11b+ Ly6C$^{low}$ Ly6G+), M1-like TAMs (CD45+CD11b+F4/80+CD86+CD206−) and M2-like TAMs (CD45+ CD11b+ F4/80+ CD86− CD206+), and Treg(CD45+CD4+CD25+FoxP3+).

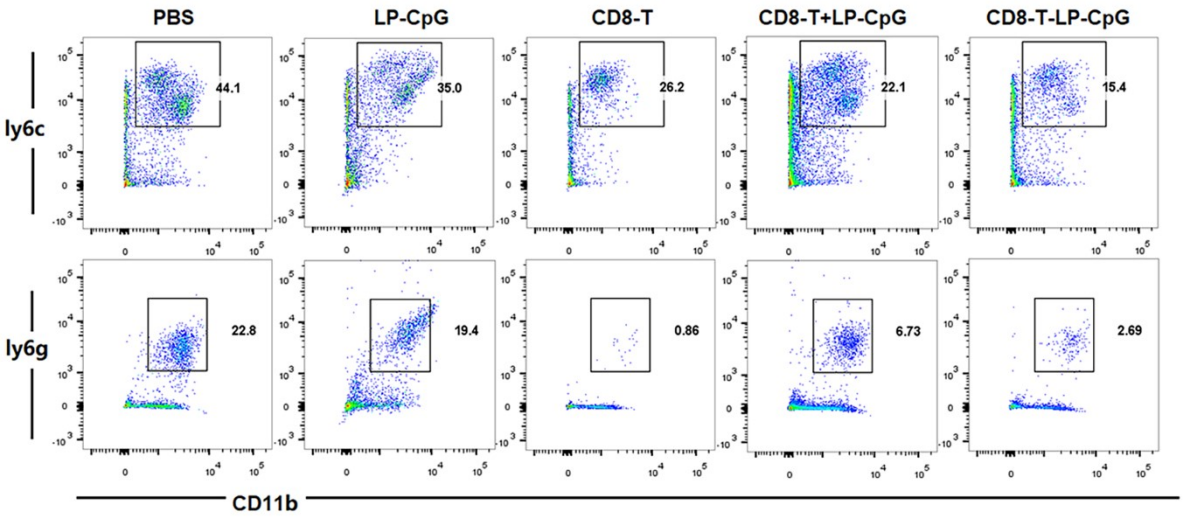

Figure S10. MDSCs fraction gated from CD45+ cells in TIL after the treatment of the following groups including PBS, LP-CpG, CD8-T, CD8-T+LP-CpG, CD8-T-LP-CpG.

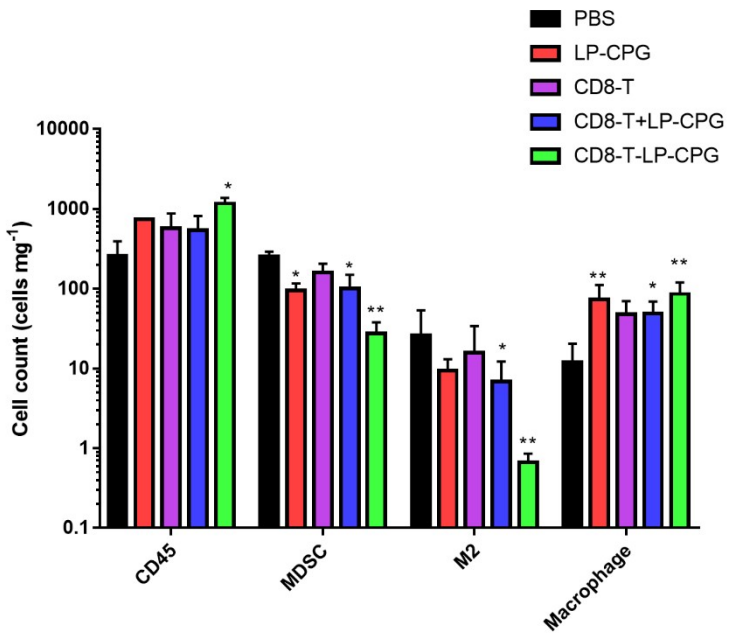


Figure S11. Flow cytometry quantification of the absolute number of lymphocyte subtypes in TIL including MDSCs, M2s, Marophages from tumor at 72h following the last treatment (n=3). *P＜0.05,**P < 0.01 by t-test.

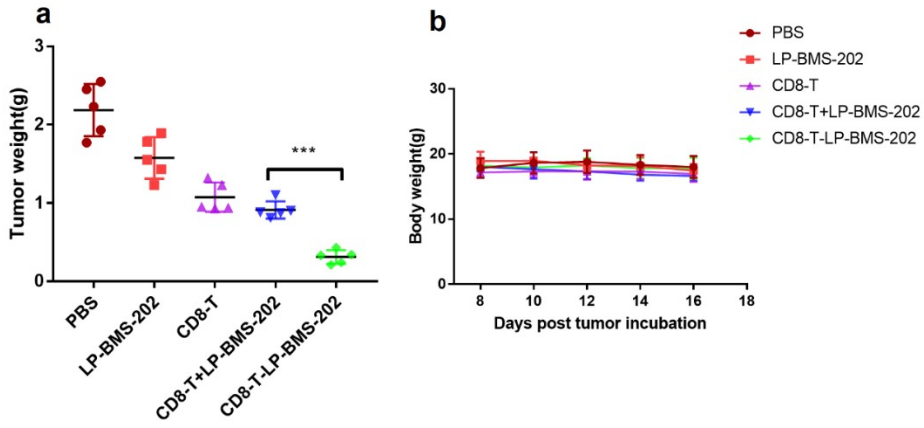


Figure S12. T Antitumor effect of OT-1 CD8-T-LP-BMS-202 in the subcutaneous B16-OVA tumor model (n=5). (a) Body weight change curves of mice; (b) Tumor weight of each group.

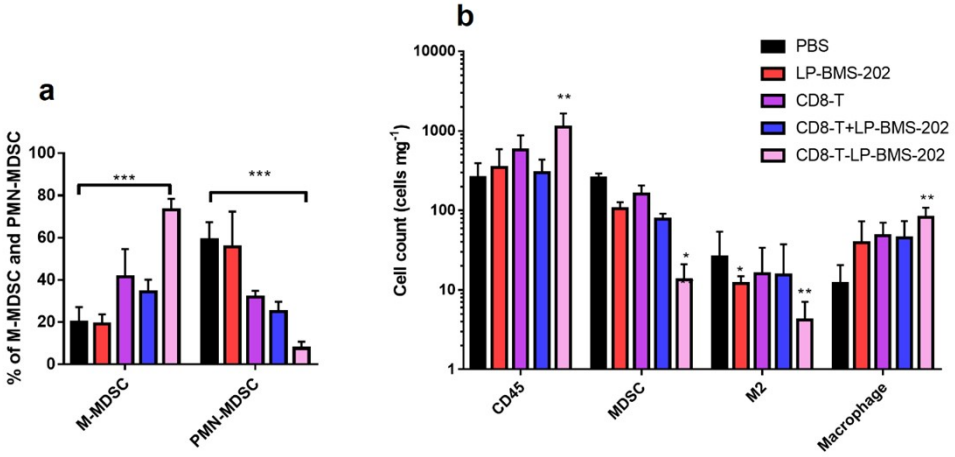


Figure S13. Immune regulation of OT-1 CD8-T-LP-BMS-202 in the subcutaneous B16-OVA tumor model. (a) Statistic results of M-MDSC and PMN-MDSC frequency in TIL; (b) Flow cytometry quantification of the absolute number of lymphocyte subtypes in TIL including MDSCs, M2-TMAs, Macrophages from tumor at 72h following the last treatment (n = 3). *P < 0.05,**P < 0.01 by t-test.

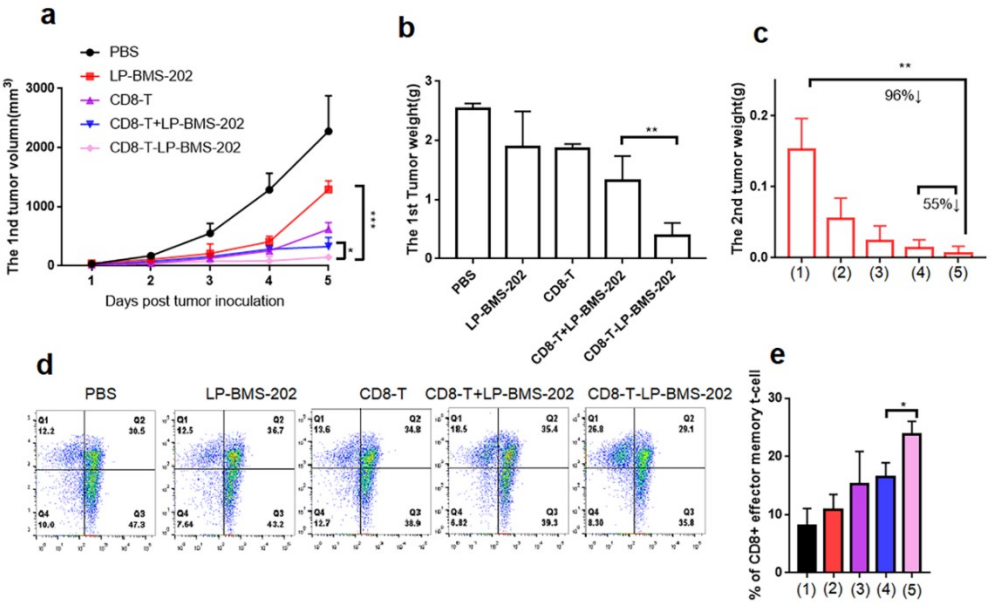


Figure S14. Immune memory establishment after treatment of all the groups including PBS, LP-BMS-202, CD8-T, CD8T+LP-BMS-202, CD8-T-LP-BMS-202 in the subcutaneous B16-OVA tumor model (n=5). (a) Treatment schedule for this assay; (b) Tumor growth curves of the 1st tumor; (c) Tumor weight of the 1st tumor; (d) Tumor weight of the 2nd tumor; (e) Determination of effector memory

T cells ($CD44^{high}$ $CD62L^{low}$) and central memory T cells ($CD44^{high}$ $CD62L^{high}$) of splenic $CD8^+$ T cells by flow cytometry; (f) Statistic analysis of effector memory T cells (n = 3).

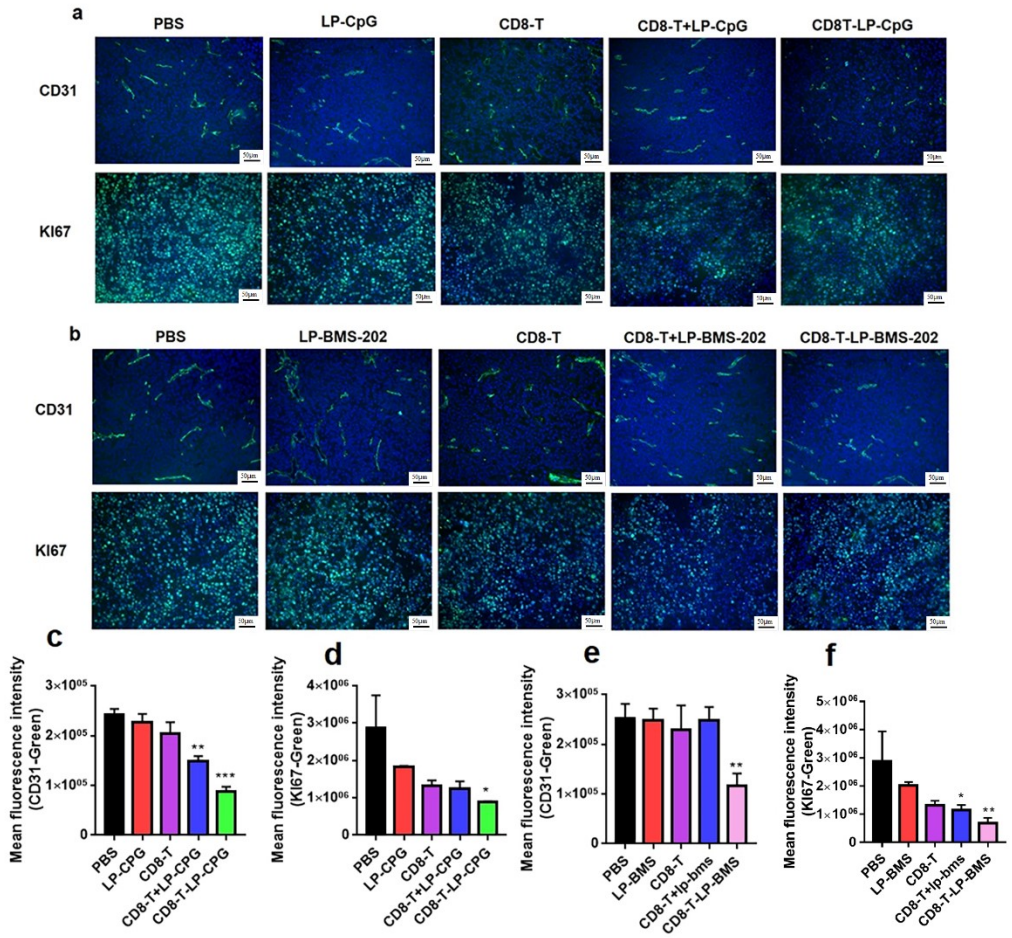


Figure S15. Inhibition of tumor angiogenesis and proliferation by CD8-T-LP-CpG(a) and CD8-T-LP-BMS-202 (b). Immunohistochemical analysis of CD31 (pan-endothelial marker) and Ki67 (proliferation marker) stained with anti-CD31 antibody (200×) and anti-KI67 antibody (200×), respectively. Blue: DAPI, Green:CD31 or KI67. Statistical results given by ImageJ (c-f) are presented as the mean ± SD, n = 3, ** $p < 0.01$, *** $p<0.001$.